9-19-2024

Lamina Cribrosa Microstructure in Nonhuman Primates With Naturally Occurring Peripapillary Retinal Nerve Fiber Layer Thinning

Palaiologos Alexopoulos

Arthur G Fernandes

Zeinab Ghassabi

Ronald Zambrano

Anse Vellappally

See next page for additional authors

Authors

Palaiologos Alexopoulos, Arthur G Fernandes, Zeinab Ghassabi, Ronald Zambrano, Anse Vellappally, Eitan Shemuelian, TingFang Lee, Jiyuan Hu, Armando Burgos-Rodriguez, Melween I Martinez, Joel S. Schuman, Amanda D Melin, James P Higham, John Danias, and Gadi Wollstein

tvst

Glaucoma

Lamina Cribrosa Microstructure in Nonhuman Primates With Naturally Occurring Peripapillary Retinal Nerve Fiber Layer Thinning

Palaiologos Alexopoulos[1], Arthur G. Fernandes[2], Zeinab Ghassabi[1], Ronald Zambrano[3], Anse Vellappally[1], Eitan Shemuelian[1], TingFang Lee[1,4], Jiyuan Hu[4], Armando Burgos-Rodriguez[5], Melween I. Martinez[5], Joel S. Schuman[3,6,7], Amanda D. Melin[2,8,9], James P. Higham[10], John Danias[11], and Gadi Wollstein[3]

[1] Department of Ophthalmology, NYU School of Medicine, New York, NY, USA
[2] Department of Anthropology & Archaeology, University of Calgary, Calgary, Alberta, Canada
[3] Wills Eye Hospital, Philadelphia, PA, USA
[4] Department of Population Health, New York University, New York, NY, USA
[5] Caribbean Primate Research Center, Universidad de Puerto Rico, San Juan, PR, USA
[6] Sidney Kimmel Medical College, Thomas Jefferson University, Philadelphia, PA, USA
[7] Drexel University, School of Biomedical Engineering, Science and Health Studies, Philadelphia, PA, USA
[8] Department of Medical Genetics, Alberta Health Services, Edmonton, Alberta, Canada
[9] Alberta Children's Hospital Research Institute, University of Calgary, Calgary, Alberta, Canada
[10] Department of Anthropology, New York University, New York, NY, USA
[11] Department of Ophthalmology & Cell Biology, SUNY Downstate Health Sciences University, Brooklyn, NY, USA

Correspondence: Gadi Wollstein, Wills Eye Hospital, 840 Walnut St., Philadelphia, PA 19107, USA.
e-mail: gwollstein@willseye.org

Received: November 16, 2023
Accepted: July 31, 2024
Published: September 19, 2024

Keywords: optical coherence tomography (OCT); lamina cribrosa (LC); retinal nerve fiber layer (RNFL)

Citation: Alexopoulos P, Fernandes AG, Ghassabi Z, Zambrano R, Vellappally A, Shemuelian E, Lee T, Hu J, Burgos-Rodriguez A, Martinez MI, Schuman JS, Melin AD, Higham JP, Danias J, Wollstein G. Lamina cribrosa microstructure in nonhuman primates with naturally occurring peripapillary retinal nerve fiber layer thinning. Transl Vis Sci Technol. 2024;13(9):23, https://doi.org/10.1167/tvst.13.9.23

Purpose: The lamina cribrosa (LC) is hypothesized to be the site of initial axonal damage in glaucoma with the circumpapillary retinal nerve fiber layer thickness (RNFL-T) widely used as a standard metric for quantifying the glaucomatous damage. The purpose of this study was to determine in vivo, 3-dimensional (3D) differences in the microstructure of the LC in eyes of nonhuman primates (NHPs) with naturally occurring glaucoma.

Methods: Spectral-domain optical coherence tomography (OCT) scans (Leica, Chicago, IL, USA) of the optic nerve head were acquired from a colony of 50 adult rhesus monkeys suspected of having high prevalence of glaucoma. The RNFL-T was analyzed globally and in quadrants using a semi-automated segmentation software. From a set of 100 eyes, 18 eyes with the thinnest global RNFL-T were selected as the study group and 18 eyes with RNFL-T values around the 50th percentile were used as controls. A previously described automated segmentation algorithm was used for LC microstructure analysis. Parameters included beam thickness, pore diameter and their ratio (beam-to-pore ratio [BPR]), pore area and shape parameters, beam and pore volume, and connective tissue volume fraction (CTVF; beam volume/total volume). The LC microstructure was analyzed globally and in the following volumetric sectors: quadrants, central and peripheral lamina, and three depth slabs (anterior, middle, and posterior).

Results: Although no significant difference was detected between groups for age, weight, or disc size, the study group had significantly thinner RNFL than the control group ($P < 0.01$). The study group had significantly smaller global and sectoral pore diameter and larger BPR compared with the control group. Across eyes, the global RNFL-T was associated positively with pore diameter globally. BPR and CTVF were significantly and negatively associated with the corresponding RNFL-T in the superior quadrant.

Conclusions: Global and sectoral microstructural differences were detected when comparing thin and normal RNFL-T eyes. Whether these LC differences are the cause of RNFL damage or the result of remodeling of the LC requires further investigation.

Translational Relevance: Our findings indicate structural alterations in the LC of NHP exhibiting natural thinning of the RNFL, a common characteristic of glaucomatous damage.

Introduction

Glaucoma is an optic neuropathy that is characterized by distinct patterns of damage in visual function and in the structure of the optic nerve head (ONH) and retina. The lamina cribrosa (LC) within the ONH has been suggested to play an important role in glaucoma pathogenesis,[1] as it has been shown to exhibit structural vulnerabilities compared with other regions of the eye.[2] Studies of the LC microstructure were previously possible ex vivo using histological samples or, when examined in vivo, have been primarily focused on the anterior LC surface. With advancements in optical coherence tomography (OCT) imaging and image processing, it is now possible to thoroughly study in vivo the full depth of the LC, allowing for detailed 3-dimensional (3D) analysis.[3,4]

The most commonly used metric to quantify structural glaucomatous damage is the thickness of the axons of the retinal ganglion cells, measured as the circumpapillary retinal nerve fiber layer thickness (RNFL-T). The axons enter the ONH and pass through the LC on their course to the brain in a spatial organization.[5] In this study, we use in vivo 3D visualization of the LC to investigate the relationship between structural changes in the retina and the LC.

Nonhuman primates (NHPs) are a preferred animal model for glaucoma studies because their eye anatomy (including the LC) and their visual pathway highly resemble those of humans.[6] A cohort of rhesus macaque NHPs has been previously described to show naturally occurring glaucoma-like disease in a colony of free-ranging animals on the island of Cayo Santiago, off the coast of Puerto Rico.[7] These animals offer a unique opportunity of assessing the natural trajectory of glaucoma without the confounding factors commonly present in human studies, such as intraocular pressure (IOP) lowering treatment and varying environmental conditions, such as nutrition. Other animal models of glaucoma often involve the induction of chronic IOP elevation leading to subsequent structural changes akin to those observed in glaucoma but lack the underlying compilation of glaucomatous properties, such as the biomechanical characteristics, vasculature, genetics, and other underlying factors. This cohort of NHPs with naturally occurring glaucoma-like disease is an important population for studying the natural course of glaucoma.

The purpose of this study was to determine in vivo differences in the 3D LC microstructure in NHP eyes with naturally occurring thinner RNFL compared with those with normal thickness. Identifying such differences will provide an indication for the association between structural changes in the LC and RNFL-T. Furthermore, we will determine the spatial relationship between localized thinning of the RNFL and corresponding differences in the LC volume.

Methods

Rhesus macaque monkeys (*Macaca mulatta*) derived from a colony suspected of having animals with naturally occurring glaucoma were examined in this study.[7] This colony lives on the island of Cayo Santiago, off the coast of Puerto Rico. The present study population consists of animals derived from Cayo Santiago, that currently reside at the Sabana Seca Field Station (SSFS). The SSFS is a research facility where animals are socially housed in outdoor enclosures. All enclosures have perches, climbing structures, and areas protected from the weather. Monkeys are fed commercial monkey chow once daily and water is available ad libitum. The standard diet is supplemented with fresh fruit, vegetables, and browse. The population in both locations is managed by the Caribbean Primate Research Center (CPRC) of the University of Puerto Rico.

All procedures of this experiment were approved by the Institutional Animal Care and Use Committee (IACUC) of the University of Puerto Rico and New York University and adhered to both the guidelines outlined in the National Institute of Health's (NIH) Guide for the Care and Use of Laboratory Animals and the Association of Research in Vision and Ophthalmology (ARVO) statement for the use of animals in ophthalmic and vision research.

Study Design

Fifty adult rhesus macaques were examined for this project, with the sole inclusion criterion being the adequate quality of peripapillary and LC OCT images. The animals were then divided into two groups based on their RNFL-T, and a comparison of LC microstructure was conducted between these groups.

The animals were sedated using an intramuscular ketamine injection (20 mg/kg) and intravenous xylazine (0.25 mg/kg) to minimize movements. Subsequently, the animals were placed on a surgical table in a prone position. Tetracaine anesthetic drops were instilled and their IOP was measured (TonoVet Plus; iCare, Vantaa, Finland). The average time interval between ketamine injection and IOP measurement was 8 $\pm$ 2 minutes. Images of the anterior segment and fundus were then captured (TRC-NW400 Non-Mydriatic Retinal

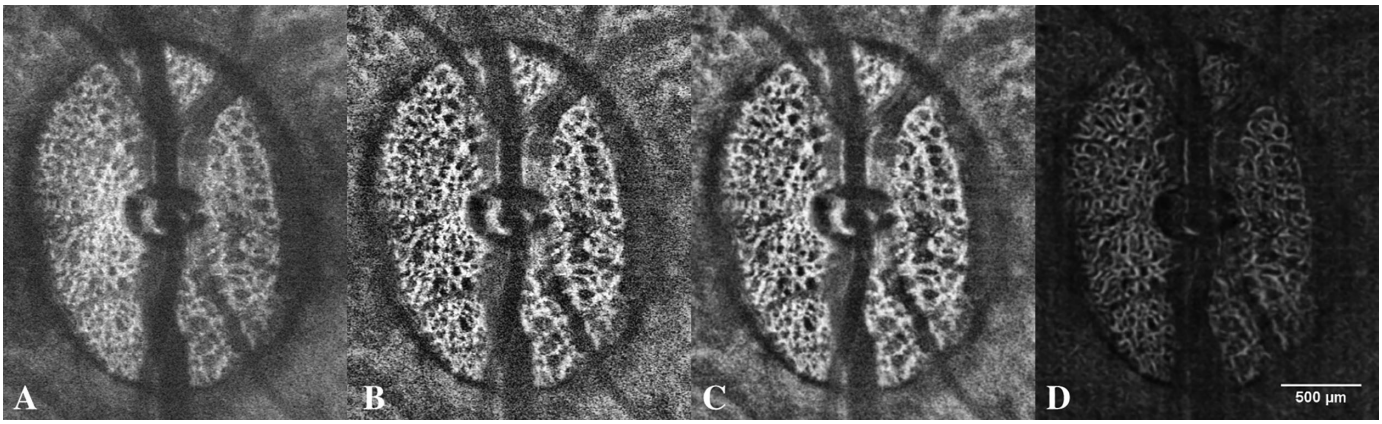

Figure 1. Pipeline of LC microstructure analysis (same pipeline performed for all LC images). (**A**) Original image (unprocessed). (**B**) Local contrast enhancement (CLAHE). (**C**) The 3D Gaussian smoothing. (**D**) Frangi's Hessian Objectness filter.

Camera; Topcon, Oakland, NJ, USA). The cup-to-disc ratio (CDR) was evaluated by two experienced raters (authors G.W. and J.D.) from the fundus photographs. All fundus images were thoroughly inspected by the same raters to exclude other apparent causes of optic neuropathies.

OCT Image Acquisition and Analysis

Spectral-domain OCT scans of the ONH region were acquired in vivo using the Bioptigen Envisu R-4310 System (Leica, Chicago, IL, USA). In the default scan configuration, the zero-delay line was adjusted to clearly visualize the inner retinal layers and scans were acquired after being centered on the ONH region. A 5 × 5 × 2 mm cubical scan was then acquired, optimized to best visualize the RNFL. For the laminar scans, enhanced depth imaging (EDI) of the ONH was acquired with the zero-delay line adjusted to enable detailed visualization of the LC, capturing a volumetric scan of the LC with 3 × 3 × 2 mm field of view.

The ONH margins were delineated based on the Bruch's membrane opening (BMO) and the geometric center of the optic nerve was automatically determined. The RNFL-T was measured from the 5 × 5 scans focused on the inner retina, at the human default sampling location, with a 1.7 mm radius from the optic nerve center using the Iowa segmentation software (Retinal Image Analysis Lab, Iowa Institute for Biomedical Imaging, Iowa City, IA, USA).[8–10] Specifically, the RNFL-T was defined as the thickness between the internal limiting membrane and the border between the RNFL and the ganglion cell layer. A 1.7 mm circle was centered on the ONH centroid. For each pixel along the sampling circle, this thickness was measured. The average RNFL-T was calculated as the mean measurement of the thickness values along the entire circle. Similarly, for the four quadrants, this value was calculated as the mean of the thickness values within each quadrant, using a method similar to that used in human scanning. Because there is no normative dataset of RNFL-T in macaques, we divided the eyes according to their RNFL-T with the lower quartile selected for analysis as the "thin RNFL group." An equal number of eyes with RNFL-T values near the 50th percentile were selected as the "normal RNFL (control) group." This approach ensured that the study sample size matched the reference size while maintaining a clear distinction between the included eyes, with no overlap. To prevent selection bias, the LC scans were visualized only after the RNFL-T based groups were determined.

The quality of each scan was assessed subjectively by an experienced rater (author P.A.) based on the clarity of the pore and beam margins prior to the performance of any quantitative analysis. The LC scans were enhanced via local contrast (CLAHE) and Gaussian smoothing in ImageJ (ImageJ, National Institutes of Health, Bethesda, MD, USA; https://imagej.nih.gov/ij/),[11] and subsequently Frangi's vesselness filter was applied (Fig. 1). The Hessian Objectness filter was applied to the volumetric scans that extracts sheet-like structures from the 3D cube, representing the LC beams. Enhancement, smoothening, and filtering were applied using the same setting across all images. The region of interest (ROI), where pores and beams are visible within the 3D cube, was manually defined for each scan by an experienced operator (author P.A.). For the LC pore segmentation, a previously described automated segmentation algorithm was used.[12] In brief, the segmentation was based upon automated pore and beam segmentation using local thresholding

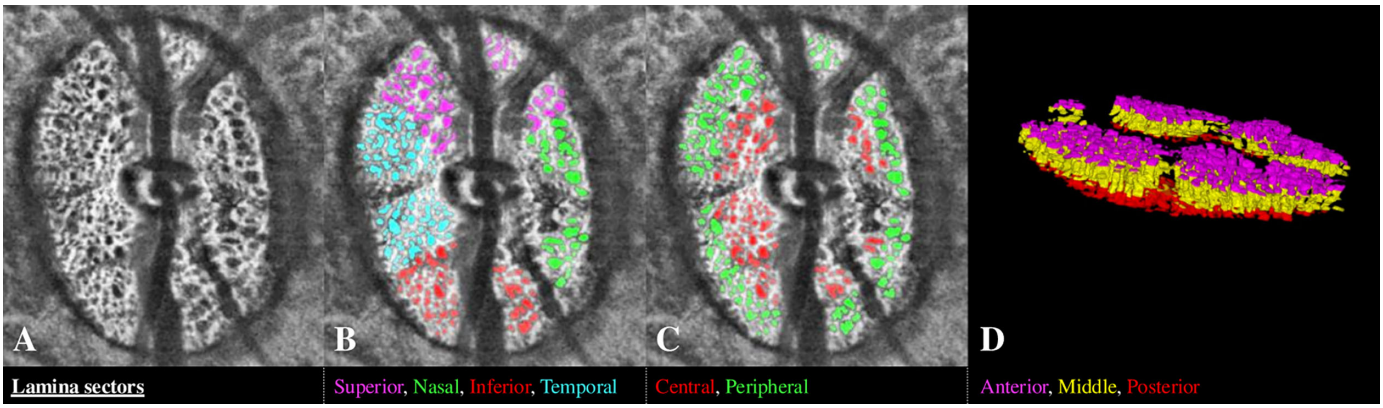

Figure 2. (**A**) En face image of the LC overlaid with (**B**) pore segmentation colored by quadrants, (**C**) cylinders, and (**D**) 3D rendering of the depth slabs.

after noise removal. Because of the complex structure of the lamina, we quantified it in the most comprehensive approach, providing both parameters obtained by 3D analysis (pore diameter, pore diameter SD, beam thickness, beam thickness SD, and beam thickness to pore diameter ratio [BPR]) and parameters averaged on sequential single-pixel-thick parallel planes (C-mode slices; pore area and pore aspect ratio) that were resampled from the scan volume. The pixel-thick slices provided the highest cross-sectional accuracy of the measurements as any averaging process of the parallel planes (for example, implementing rolling average) would subjectively improve the noise in the slices but would alter the pore-beam border, therefore adding an unpredictable factor of variability in the segmentation of the pores (which is consistent across all scans). Pore area represents the average area of each individual pore in the scan volume, whereas the pore aspect ratio represents the ratio of the major axis ("width") to the perpendicular minor axis ("height") of an ellipse fitted to each pore. Pore diameter and beam thickness were computed by determining the largest sphere that fit within the structure at any given point, a conventional method to describe complex 3D structures.[13] All pore diameters and beam thicknesses were then averaged to generate the mean values. BPR was calculated by dividing the average beam thickness of all beams to average pore diameter of all pores. The connective tissue volume fraction (CTVF) was calculated by dividing the beam volume by the total LC volume and expressed as a percentage. Pore roundness was calculated by dividing the pore outline to a best-fitting ellipse for each pore. LC visibility was calculated as the ROI volume divided by the entire LC volume. This segmentation method has been demonstrated to offer reproducible measurements of the LC microstructure.[14,15] Moreover, it has been shown to be robust against minor variations in scan quality or image parameters, such as brightness or contrast. This robustness was confirmed through a sensitivity analysis reported in a previous publication.[16]

The LC volume was analyzed in its entirety and in volumetric sectors with the following divisions (Fig. 2): (a) quadrants of 90 degrees each (superior, nasal, inferior, and temporal), (b) cylinders of equal volume (central and peripheral LC), and (c) 3 depth slabs of equal volume (anterior, middle, and posterior) obtained by dividing the visible LC equally in the axial direction. ImageJ and its associated plugin BoneJ (https://imagej.net/plugins/bonej)[17] were used to obtain 2- and 3D measurements of the pore and beam microstructure (Fig. 3).

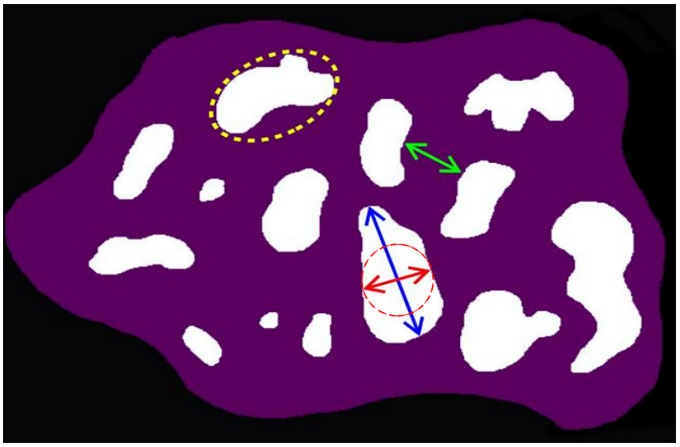

Figure 3. Parameters of the LC microstructure. Pore area (*white area*), pore diameter (*red line*), pore width (*blue arrow*) and height (*red arrow*), pore aspect ratio (*blue line/red line*), pore roundness (pore outline/*yellow ellipse*), beam thickness (*green line*), beam-to-pore ratio (BPR; average of the *green lines*/average of the *blue lines*), connective tissue volume fraction (CTVF, *purple* volume/total volume).

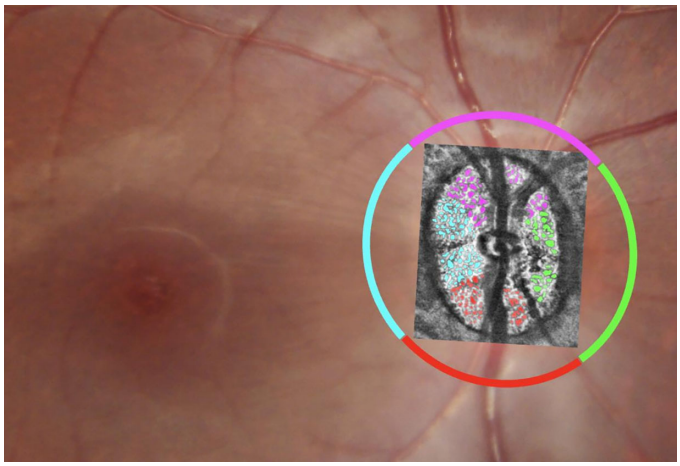

Figure 4. LC microstructure parameters were examined in four quadrants: superior (*red*), nasal (*green*), inferior (*magenta*), and temporal (*cyan*) in concordance with to RNFL quadrants.

Statistical Analysis

Mixed effect models adjusted for age, LC visibility, and scan quality were used for comparison between the thin RNFL and control groups. To examine the magnitude of the parameter differences, the values of the control group were subtracted from the thin group and divided by the overall average value of each parameter. The relative percent difference was then reported. Association between the RNFL-T and the LC parameters was tested globally and in the four corresponding quadrants (Fig. 4) using mixed effects models adjusted for age, LC visibility, and scan quality. Weight, disc area, and lamina depth were consistently nonsignificant in all models; these three parameters were therefore omitted from the final models for both groupwise comparisons and associations. R statistical package (R: A language and environment for statistical computing; R Foundation for Statistical Computing, Vienna, Austria) was used for the analysis and a P value of less than 0.05 was considered as statistically significant.

Results

One hundred eyes of 50 adult animals were used in this study. Out of the 25 eyes with the thinnest RNFL, 7 eyes were excluded due to poor LC scan quality that prohibited LC microstructure analysis and thus 18 eyes with thin RNFL and 18 control eyes from a total of 27 animals were used for the analysis (3 animals contributed both eyes to the normal thickness group, and 4 in the thin group, whereas 2 animals contributed 1 eye to each group). No statistically significant difference ($P > 0.05$) was detected between the two groups for age, weight, or optic disc area (Table 1).

Table 1. Characteristics of the Control and Thin RNFL Study Groups Reported as Mean (SD)

	Control Group	Thin RNFL Group	*P* Value
Number of eyes	18	18	
Number of animals	15	14	
Laterality (OD:OS)	11:7	9:9	0.73
Sex (M:F)	3:12	4:10	0.92
Age, y	14.8 (2.8)	13.9 (2.2)	0.75
Weight, kg	11.4 (2.6)	10.7 (3.8)	0.55
IOP, mm Hg	16.4 (0.5)	18.7 (1.0)	0.09
Disc area, mm^2	2.53 (0.05)	2.41 (0.09)	0.14
Cup-to-disc ratio	0.52 (0.03)	0.62 (0.03)	0.03
Global RNFL, µm	125.3 (0.4)	109.8 (1.3)	<0.01
Superior RNFL, µm	141.6 (1.8)	123.8 (2.6)	<0.01
Nasal RNFL, µm	99.5 (2.1)	85.7 (2.3)	<0.01
Inferior RNFL, µm	161.1 (3.1)	144.7 (3.1)	<0.01
Temporal RNFL, µm	98.6 (2.3)	85.0 (2.3)	<0.01

RNFL, retinal nerve fiber layer.

The thin RNFL group had a significantly thinner RNFL than the control group globally and in all quadrants ($P < 0.01$). The eyes in this group exhibited some typical glaucoma-like features, such as marginally significant higher IOP (18.7 vs. 16.4 mm Hg, $P = 0.09$), enlarged cupping (0.62 vs. 0.52, $P = 0.03$), and RNFL wedge defects as seen on fundus pictures; however, these features were not considered for inclusion in the study or control group but rather observational outcomes.

Groupwise Comparison of LC Parameters

When comparing the lamina parameters between the two groups, no significant difference was detected in the analyzable LC ($P = 0.53$). LC microstructure parameters in the control and thin RNFL groups are presented in Tables 2 and 3, respectively. Mean pore diameter was significantly smaller in the thin RNFL group versus the control group globally ($P < 0.01$) and across all sectors ($P \leq 0.01$). BPR was significantly higher in the thin RNFL group than the control group globally and in all sectors except the inferior and temporal quadrants. Pore shape displayed inconsistent trends with the nasal quadrant in the thin RNFL group having significantly greater mean pore aspect ratio (AR) and lesser mean pore roundness

Table 2. LC Microstructure in the Control Group Reported as Mean (SD)

	Beam Thickness	Pore Diameter	BPR	CTVF	Mean Pore AR	Mean Pore Roundness	Mean Pore Area
Global	31.89 (2.49)	28.16 (1.15)	1.13 (0.07)	63.86 (2.87)	1.97 (0.15)	0.58 (0.03)	2203 (412)
Quadrants							
Superior	29.74 (3.26)	27.14 (2.02)	1.09 (0.07)	64.34 (3.38)	1.98 (0.13)	0.57 (0.03)	1922 (477)
Nasal	32.24 (2.54)	29.54 (2.05)	1.09 (0.07)	63.44 (2.74)	1.97 (0.15)	0.57 (0.03)	2322 (428)
Inferior	28.95 (3.86)	26.01 (2.51)	1.11 (0.09)	63.93 (3.12)	2.02 (0.14)	0.56 (0.03)	1899 (427)
Temporal	31.93 (2.51)	27.03 (1.09)	1.18 (0.08)	64.12 (3.00)	1.99 (0.15)	0.57 (0.03)	1965 (412)
Cylinders							
Central	31.9 (2.72)	27.90 (1.36)	1.14 (0.07)	64.02 (2.85)	1.98 (0.13)	0.57 (0.03)	1935 (290)
Periphery	30.22 (2.12)	27.15 (1.16)	1.11 (0.07)	63.65 (2.93)	2.05 (0.12)	0.56 (0.03)	1952 (392)
Depth							
Anterior	30.84 (2.42)	26.95 (1.22)	1.14 (0.08)	63.57 (3.14)	1.98 (0.15)	0.57 (0.03)	2141 (491)
Middle	33.01 (2.66)	28.97 (1.41)	1.14 (0.07)	63.96 (2.76)	1.96 (0.15)	0.58 (0.03)	2225 (404)
Posterior	32.17 (2.68)	28.77 (1.26)	1.12 (0.08)	64.11 (2.93)	1.96 (0.16)	0.57 (0.03)	2228 (424)

AR, aspect ratio; BPR, beam-to-pore ratio; CTVF, connective tissue volume fraction; RNFL, retinal nerve fiber layer.

($P = 0.01$ for both parameters). Mean pore roundness was marginally significantly smaller in the temporal quadrant in the thin RNFL group compared to the control group ($P = 0.05$). Mean pore area and beam thickness did not differ significantly between the two groups globally or in any sector.

When evaluating locations exhibiting the maximal difference in LC parameters between the two groups, the nasal quadrant showed the largest and significant change among the quadrants for pore diameter, mean pore AR, and mean pore roundness (Table 4). For pore diameter, the difference in the nasal quadrant was significantly greater than the superior and temporal quadrants ($P < 0.01$ for both). For BPR, the largest difference was in the superior quadrant and it was significantly greater than the temporal quadrant ($P = 0.01$). The peripheral cylinder showed a larger difference in pore diameter compared to the central cylinder, whereas the opposite order was observed for BPR. Among the depth slabs, the anterior LC displayed the largest difference in pore diameter and BPR.

Association Between RNFL-T and LC Parameters

Global RNFL-T had a significant positive association with pore diameter (Table 5; Fig. 5, top). Superior BPR and CTVF were the only sectoral parameters that had a significant (negative) association with the respective RNFL thickness ($P = 0.02$ and $P = 0.05$, respectively; see Fig. 5, bottom).

Discussion

The goal of the present study was to compare in vivo 3D LC microstructure in NHP with thinning of the RNFL compared with eyes with normal RNFL thickness from a cohort of animals with high prevalence of naturally occurring glaucoma. As an indicator of potential glaucomatous damage, we focused on the commonly used clinical biomarker of RNFL-T and compared the 3D microstructure of the LC in eyes with the thinnest RNFL to eyes with average RNFL thickness. The main difference between the groups was a larger BPR and smaller mean pore diameter in the thin RNFL group. When examining the different sectors of the lamina, these differences were noted globally and in nearly all volumetric sectors, highlighting a widespread structural involvement of the LC in the glaucomatous process.

In contrast to other animal studies investigating the lamina role in glaucoma, which include glaucoma-like changes induced by altering certain feature associated with the disease (such as IOP elevation or genetic manipulation) without having the full glaucomatous background, some of the animals in our cohort spontaneously developed glaucoma-like features. These animals exhibit a natural profile of glaucoma characteristics, including elevated IOP, large cupping, and RNFL wedge defects. Nonetheless, there was no significant difference between the tested groups in terms of age or gender, which could potentially confound the structural outcome. Additionally, all

Table 3. LC Microstructure Values in the Thin RNFL Group Reported as Mean (SD)

	Beam Thickness (µm)	*P* Value[a]	Pore Diameter (µm)	*P* Value[a]	BPR	*P* Value[a]	CTVF (%)	*P* Value[a]	Mean Pore AR	*P* Value[a]	Mean Pore Roundness	*P* Value[a]	Mean Pore Area (µm^2)	*P* Value[a]
Global	32.12 (3.74)	0.95	**26.19 (1.90)**[b]	**<0.01**	**1.23 (0.12)**[b]	**0.02**	66.27 (4.25)	0.17	2.04 (0.16)	0.10	0.56 (0.04)	0.10	2207 (574)	0.72
Quadrants														
Superior	31.99 (3.75)	0.48	**26.33 (2.09)**[b]	**<0.01**	1.22 (0.13)	0.10	66.73 (4.39)	0.41	2.03 (0.16)	0.07	0.56 (0.03)	0.09	2000 (528)	0.93
Nasal	30.38 (4.99)	0.33	**25.63 (3.24)**[b]	**<0.01**	**1.19 (0.12)**[b]	**0.01**	66.05 (4.19)	0.13	**2.10 (0.17)**[b]	**0.01**	**0.55 (0.04)**[b]	**0.01**	2290 (533)	0.74
Inferior	29.05 (4.39)	0.87	**24.26 (2.38)**[b]	**<0.01**	**1.19 (0.11)**[b]	**0.03**	66.71 (4.18)	0.09	2.08 (0.21)	0.15	0.55 (0.04)	0.17	1823 (530)	0.78
Temporal	32.11 (3.42)	0.68	**25.52 (2.07)**[b]	**0.01**	1.26 (0.13)	0.08	66.16 (4.47)	0.33	2.08 (0.16)	0.06	**0.55 (0.03)**[b]	**0.05**	1957 (543)	0.49
Cylinders														
Central	32.30 (3.75)	0.67	**26.00 (1.72)**[b]	**<0.01**	**1.24 (0.12)**[b]	**0.02**	66.35 (4.23)	0.25	2.06 (0.15)	0.07	0.56 (0.03)	0.07	1951 (441)	0.56
Periphery	29.92 (3.47)	0.75	**25.19 (2.11)**[b]	**<0.01**	**1.19 (0.10)**[b]	**0.02**	66.04 (4.24)	0.16	2.13 (0.17)	0.07	0.54 (0.03)	0.08	1931 (439)	0.87
Depth														
Anterior	31.04 (2.96)	0.94	**24.98 (2.11)**[b]	**<0.01**	**1.25 (0.14)**[b]	**0.01**	66.14 (4.75)	0.10	2.03 (0.15)	0.30	0.56 (0.03)	0.23	2121 (667)	0.97
Middle	33.78 (4.63)	0.70	**27.25 (2.26)**[b]	**<0.01**	**1.24 (0.12)**[b]	**0.02**	66.19 (3.98)	0.18	2.04 (0.16)	0.07	0.56 (0.04)	0.09	2265 (536)	0.57
Posterior	32.65 (3.91)	0.73	**26.92 (2.12)**[b]	**<0.01**	**1.21 (0.12)**[b]	**0.04**	66.69 (4.32)	0.21	2.03 (0.19)	0.09	0.56 (0.04)	0.07	2220 (681)	0.64

AR, aspect ratio; BPR, beam-to-pore ratio; CTVF, connective tissue volume fraction; RNFL, retinal nerve fiber layer.
The *P* values for groupwise comparison of each parameter with the corresponding value in the control group (Table 2) are reported in subsequent columns.
[a]The *P* value for comparison with the control group (Table 2).
[b]Significant difference in bold face ($P < 0.05$).

Table 4. Relative Differences in LC Microstructure Parameters Between the Thin RNFL and Control Groups

	Beam Thickness	Pore Diameter	BPR	CTVF	Mean Pore AR	Mean Pore Roundness	Mean Pore Area
Global	+0.74%	**−7.23%**[a]	**+8.05%**[a]	+3.70%	+3.53%	−2.76[a]	+0.18%
Quadrants							
Superior	+7.27%	**−3.04%**[a]	**+10.60%**[b]	+3.64%	+2.40%	−1.44%	+3.98%
Nasal	−5.95%	**−14.16%**[a,c]	**+8.14%**[a]	+4.04%	**+6.30%**[a]	**−4.99%**[a]	+6.30%
Inferior	+0.33%	**−6.97%**[a]	+7.15%	+4.24%	+2.85%	−1.79%	−4.09%
Temporal	+0.58%	**−5.73%**[a]	+6.58%	+3.14%	+4.41%	**−3.68%**[a]	−0.41%
Cylinders							
Central	+1.24%	**−7.04%**[a]	**+8.39%**[a]	+3.58%	+3.87%	−2.98%	+0.84%
Periphery	−1.03%	**−7.46%**[a]	**+6.43%**[a]	+3.68%	+3.60%	−2.66%	−1.08%
Depth							
Anterior	+0.64%	**−7.58%**[a]	**+8.69%**[a]	+3.96%	+2.59%	−2.20%	−0.93%
Middle	+2.28%	**−6.11%**[a]	**+8.29%**[a]	+3.42%	+4.11%	−3.08%	+1.77%
Posterior	+1.50%	**−6.65%**[a]	**+8.28%**[a]	+3.95%	+3.36%	−2.67%	−0.38%

AR, aspect ratio; BPR, beam-to-pore ratio; CTVF, connective tissue volume fraction; RNFL, retinal nerve fiber layer.
Positive values mark parameters which are larger in the thin RNFL group.
[a]Significant difference ($p < 0.05$);
[b]Significant difference ($p < 0.05$) compared to temporal quadrant;
[c]Significant difference ($p < 0.05$) compared to superior, temporal quadrants.

Table 5. Associations Between RNFL Thickness and LC Microstructure Parameters

	Beam Thickness (μm)	Pore Diameter (μm)	BPR	CTVF	Mean Pore AR	Mean Pore Roundness	Mean Pore Area (μm^2)
Global	0.39	**1.37**[a]	−6.55	−6.68	−4.06	19.53	−0.0014
	$P = 0.16$	$\mathbf{P < 0.01}$	$P = 0.43$	$P = 0.77$	$P = 0.27$	$P = 0.25$	$P = 0.29$
Quadrants							
Superior	−0.72	1.28	**−38.26**[a]	**−92.87**[a]	4.82	−31.71	0.0056
	$P = 0.17$	$P = 0.17$	$\mathbf{P = 0.02}$	$\mathbf{P = 0.05}$	$P = 0.66$	$P = 0.53$	$P = 0.12$
Nasal	0.44	0.24	−10.81	−20.81	−6.24	28.82	−0.0026
	$P = 0.09$	$P = 0.37$	$P = 0.29$	$P = 0.46$	$P = 0.17$	$P = 0.14$	$P = 0.25$
Inferior	−0.17	−0.04	−11.82	−4.45	−0.53	35.85	−0.0051
	$P = 0.75$	$P = 0.96$	$P = 0.57$	$P = 0.94$	$P = 0.96$	$P = 0.50$	$P = 0.11$
Temporal	0.33	1.03	−6.48	−11.01	−10.40	46.09	−0.0003
	$P = 0.49$	$P = 0.16$	$P = 0.59$	$P = 0.75$	$P = 0.15$	$P = 0.17$	$P = 0.90$

AR, aspect ratio; BPR, beam-to-pore ratio; CTVF, connective tissue volume fraction; RNFL, retinal nerve fiber layer.
[a]Significant association in bold face ($P < 0.05$).
Each estimate represents the effect of a unit change for each parameter on the RNFL thickness.

animals were selected from a single population in a confined, shared environment. Therefore, environmental factors, such as nutrition or sun-light exposure, are not expected to have an impact on our findings.

The in vivo nature of our study precludes histological validation of glaucoma. However, a prior study involving an animal from this island exhibiting enlarged cupping revealed a significant reduction in axonal count in the affected eye, consistent with characteristics indicative of glaucomatous damage.[7] An additional novel aspect of our study is the automated 3D analysis of the entire lamina microstructure, throughout the entire visible laminar depth. A prior study highlighted the inadequacy of

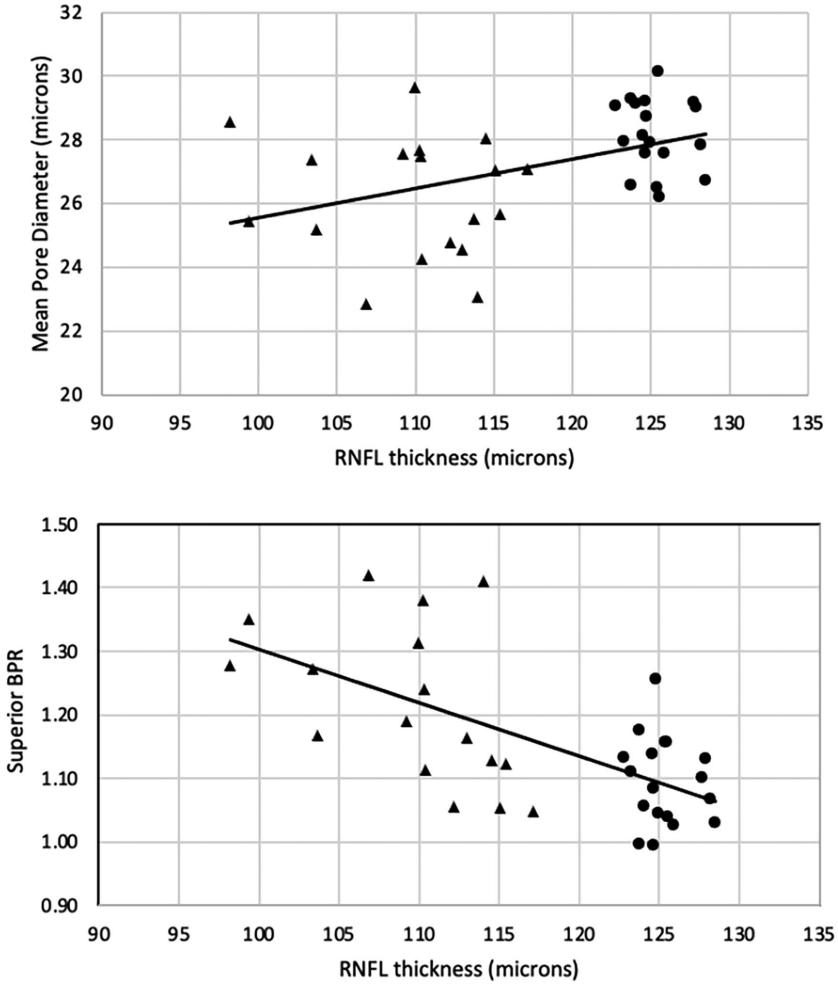

Figure 5. Associations between global RNFL thickness and mean pore diameter (top) and superior BPR (bottom). Triangles: Thin RNFL group, Circles: Normal RNFL thickness group. RNFL: Retinal nerve fiber layer thickness, BPR: Beam to pore ratio.

exclusively focusing on the anterior surface of the lamina, a common approach in LC research; this limited approach fails to fully capture the changes occurring within the depth of the lamina, potentially leading to deleterious impact on the axons passing through it.[18] The 3D method of calculating beam and pore thickness via calculating the local thickness by implementing the largest sphere for each voxel has been extensively validated and widely used in scientific research, particularly in fields such as materials science and biomedical engineering.[19,20] Studies like those by Hildebrand and Rüegsegger (1997)[21] have demonstrated its effectiveness in characterizing the thickness of trabecular bone and other porous structures. The method provides a consistent and objective measure of local thickness, given that it is mathematically robust and well-defined, crucial characteristics for comparative analysis across samples. According to the articles above it is particularly useful in complex structures, such as the LC with many local variations in thickness. Specifically for LC studies, this metric has been used by other authors in the field for similar calculations.[22,23]

Our finding of higher BPR in NHP eyes with thinner RNFL compared to control eyes is in agreement with a previous study documenting the same finding in glaucomatous compared to healthy humans eyes.[24] Being a ratio between two of the main features of the lamina (beam thickness and pore diameter), BPR is considered a robust structural biomarker, which compared to other LC parameters is less affected by magnification, scanning angle, and other potential confounders. An increase in BPR can be driven by either an increase in the beam thickness or a decrease in pore diameter. We demonstrated that the difference in BPR values was mostly driven by a significant decrease in pore diameter while no significant difference was noted for beam thickness globally or in any sectors.

Lower pore diameter might be the cause for strangulating RGC axons that leads to their death and thinning of the RNFL. Alternatively, this might be the outcome of the LC remodeling due to the primary axonal loss. Further longitudinal studies are warranted to determine the causation.

Alterations of lamina microstructure in glaucomatous eyes have been reported in the literature, although the reports on changes in pore size do not follow a consistent pattern. Ivers et al. documented larger pores in NHP eyes with experimental glaucoma in the superotemporal and inferotemporal regions of the anterior lamina surface.[25] Similar findings were also reported by Vilupuru et al. in an NHP experimental glaucoma study where adaptive optics – scanning laser ophthalmoscopy imaging was used.[26] However, in both studies, only the pores of the anterior LC surface were examined, as opposed to the full 3D analysis of the present study. The expansion of pores in the anterior surface can be attributed to the influence of IOP on the anterior laminar surface, resulting in localized stretching of the pores. Pore diameter was also larger in an ex vivo study by Reynaud et al. of NHPs with experimental glaucoma, although these eyes displayed increased CTVF, a finding that corresponds to our results.[23] Contradicting findings were reported by Wang et al. in an in vivo study of human glaucomatous and healthy eyes where decreased pore diameter was associated with worsening of visual field damage.[24] This has been also reported by Omokada et al., who analyzed the entire LC depth of a small sample of human glaucomatous and healthy eyes, and found that glaucomatous eyes had smaller pores in terms of both 3D volume as well as cross-sectional area.[27] Studies focusing on the LC microstructure differences between heathy and glaucoma (or glaucoma-like) eyes use different study designs, technologies, and analysis tools, yielding inconsistent findings regarding the pore size differences in glaucoma.

It should be noted that the inherent properties of OCT and the changes occurring in the tissue in glaucoma-like eyes might confound the quantified differences from healthy eyes due to two main factors: (1) the presence of thick prelaminar tissue in healthy eyes can reduce LC image quality, thus affecting measurements, and (2) the posterior displacement of the LC within glaucomatous optic nerves, compared to healthy eyes, can lead to an overall magnification error. Prior to any analysis, all scans used in our study underwent assessment for sufficient quality to ensure the reliability of the segmentation process, and the outcome of the analysis. Additionally, as we reported in Table 1, no significant difference was detected in disc areas between the groups. In Table 4, we reported a relative difference in microstructural parameters, with a smaller pore diameter in the thin RNFL group compared to the normal thickness group, both globally and in all sectors. Conversely, beam diameter was predominantly larger in the thin RNFL group, and the mean pore area varied across different sectors. Therefore, there is no evidence to suggest that these potential confounders significantly affected our findings.

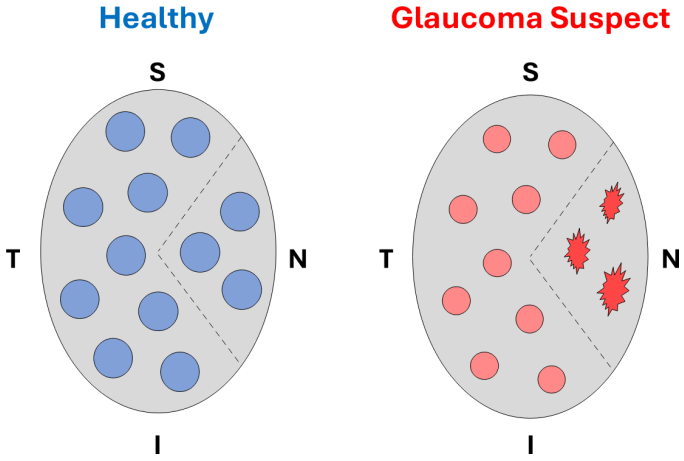

Figure 6. LC Microstructure models of healthy and suspected glaucomatous eyes. Laminar pores are displayed in the healthy LC (*blue* fill) and suspected glaucomatous LC (*red* fill) along with the beams (*gray* background). In the suspected glaucomatous eyes, the pores appear smaller in diameter and the connective tissue content is increased relative to the pores. In the nasal quadrant, the pores have increased AR (becoming more slit-like) and decreased roundness (irregular shape). I, inferior; N, nasal; S, superior; and T, temporal.

Given the intricate 3D structure of the LC, a comprehensive analysis necessitates the characterization of multiple features, as similar numerical outcomes may arise from distinct structural shapes. We noted significant differences between the groups in pore diameter, BPR, mean pore AR, and mean pore roundness across various sectors. These diverse variations underscore the robustness of the changes observed in the LC of eyes with thin RNFL. In the nasal quadrant, the pores had increased AR and decreased roundness, suggesting that the pores had a slit-like formation and more irregular shape. At the same time, the pores were smaller, as evidenced by the decreased pore diameter. These differences in pore size and shape were the largest in the nasal quadrant, compared to the other quadrants (see Table 4), as illustrated in Figure 6. This difference in pore diameter was significantly greater nasally compared to superiorly and temporally. According to this finding, the nasal LC is experiencing the largest structural changes in the early stages of glaucoma.

Similar LC differences have been reported in human eyes with severe to end-stage visual field loss, with

glaucomatous eyes displaying more elongated pores with decreased circularity and less regular contour. These have also been documented in NHPs with experimental glaucoma.[25,28] The cross-sectional nature of the present and other studies can only provide speculations as to whether changes in pore morphology are related to remodeling of the LC causing axonal compression, focal damage, or loss of axons leading to tissue expansion and pore shrinkage.

When testing the association between lamina parameters and retinal parameters, there was a significant positive association between global RNFL-T and pore diameter (thinner RNFL associated with smaller pore diameter, and vice versa; see Fig. 5). This finding corresponds to the smaller pore diameter we reported above in the thin RNFL group in comparison to the control group. In the superior quadrant, there was a significant negative association between RNFL-T and both BPR and CTVF. The reason for the predilection to the superior quadrant is not entirely clear and may be related to the high prevalence of early glaucomatous damage occurring in this region,[29] which provides a larger spread of the measurements and improves the possibility of detecting correlations. Although these findings may appear to contradict observations in human eyes, where early glaucomatous changes often manifest in the temporal superior and temporal inferior regions, these findings pertain to the optic nerve head cupping and peripapillary region with paucity of information of in vivo changes occurring in the LC at an early stage of glaucoma. Additionally, these differences may also reflect inter-species variations. Wang et al. reported that worsening of disease functionally, as recorded by visual field mean deviation (VF MD), was associated with decreased pore area and diameter and increased beam thickness and BPR.[24] This might indicate that the changes in the LC are proportional not only to the structural changes in the RNFL thickness but also to the ocular function. Further investigation is warranted.

Some limitations of the study should be acknowledged. Because this is an in vivo NHP study, we cannot definitively attribute the thinning of the RNFL to glaucomatous damage. However, our primary objective was to examine the association between RNFL thickness and the corresponding LC structure and the presence of animals with glaucoma-like disease in the tested cohort enhances our analysis by broadening the variability in RNFL thickness. Additionally, the limited visibility of the LC is a common constraint of OCT technology. This inherent limitation of OCT technology is partially addressed by aggregating data across multiple eyes, particularly when the analyzable area varied, thereby enabling coverage of larger areas of the lamina. Finally, whereas the 3D approach to calculating pore and diameter thickness is widely used, it is not sufficient by itself to fully describe the highly complex structure of pores and beams in space.

In conclusion, we demonstrated microstructural LC differences both global and sectoral in NHP eyes with thin RNFL compared with the control group. This provides further insight into the involvement of the LC in the glaucomatous process. Further longitudinal investigations are required to determine whether these differences are the cause or the effect of the disease.

Acknowledgments

Supported by the NIH R01-EY030770, NIH R01-EY035174, and R01-EY013178, New Frontiers in Research Fund NFRFE-2018-02159, the National Glaucoma Research program, the BrightFocus Foundation (Grant no. G2020047), and the Natural Sciences and Engineering Research Council of Canada (RGPIN-2017-03782), P40OD012217.

Disclosure: **P. Alexopoulos**, None; **A.G. Fernandes**, None; **Z. Ghassabi**, None; **R. Zambrano**, None; **A. Vellappally**, None; **E. Shemuelian**, None; **T. Lee**, None; **J. Hu**, None; **A. Burgos-Rodriguez**, None; **M.I. Martinez**, None; **J.S. Schuman**, receives royalties for intellectual property licensed by Massachusetts Institute of Technology and Massachusetts Eye and Ear Infirmary to Zeiss (R); **A.D. Melin**, None; **J.P. Higham**, None; **J. Danias**, None; **G. Wollstein**, None

References

1. Andrade JCF, Kanadani FN, Furlanetto RL, Lopes FS, Ritch R, Prata TS. Elucidation of the role of the lamina cribrosa in glaucoma using optical coherence tomography. *Surv Ophthalmol*. 2022;67(1):197–216.
2. Downs JC, Girkin CA. Lamina cribrosa in glaucoma. *Curr Opin Ophthalmol*. 2017;28(2):113–119.
3. Park SC, De Moraes CG, Teng CC, Tello C, Liebmann JM, Ritch R. Enhanced depth imaging optical coherence tomography of deep optic nerve complex structures in glaucoma. *Ophthalmology*. 2012;119(1):3–9.
4. Park HY, Park CK. Diagnostic capability of lamina cribrosa thickness by enhanced depth imaging and factors affecting thickness in patients with glaucoma. *Ophthalmology*. 2013;120(4):745–752.

5. Radius RL, Anderson DR. The course of axons through the retina and optic nerve head. *Arch Ophthalmol*. 1979;97(6):1154–1158.
6. Picaud S, Dalkara D, Marazova K, Goureau O, Roska B, Sahel JA. The primate model for understanding and restoring vision. *Proc Natl Acad Sci USA*. 2019;116(52):26280–26287.
7. Dawson WW, Brooks DE, Hope GM, et al. Primary open angle glaucomas in the rhesus monkey. *Br J Ophthalmol*. 1993;77(5):302–310.
8. Abràmoff MD, Garvin MK, Sonka M. Retinal imaging and image analysis. *IEEE Rev Biomed Eng*. 2010;3:169–208.
9. Garvin MK, Abràmoff MD, Wu X, Russell SR, Burns TL, Sonka M. Automated 3-D intraretinal layer segmentation of macular spectral-domain optical coherence tomography images. *IEEE Trans Med Imaging*. 2009;28(9):1436–1447.
10. Li K, Wu X, Chen DZ, Sonka M. Optimal surface segmentation in volumetric images–a graph-theoretic approach. *IEEE Trans Pattern Anal Mach Intell*. 2006;28(1):119–134.
11. Schindelin J, Arganda-Carreras I, Frise E, et al. Fiji: an open-source platform for biological-image analysis. *Nat Methods*. 2012;9(7):676–682.
12. Nadler Z, Wang B, Wollstein G, et al. Automated lamina cribrosa microstructural segmentation in optical coherence tomography scans of healthy and glaucomatous eyes. *Biomed Opt Express*. 2013;4(11):2596–2608.
13. Dougherty RP, Kunzelmann KH. Computing local thickness of 3D structures with ImageJ. *Microsc Microanal*. 2007;13:1678–1679.
14. Wang B, Nevins JE, Nadler Z, et al. Reproducibility of in-vivo OCT measured three-dimensional human lamina cribrosa microarchitecture. *PLoS One*. 2014;9(4):e95526.
15. Nadler Z, Wang B, Wollstein G, et al. Repeatability of in vivo 3D lamina cribrosa microarchitecture using adaptive optics spectral domain optical coherence tomography. *Biomed Opt Express*. 2014;5(4):1114–1123.
16. Sainulabdeen A, Glidai Y, Wu M, et al. 3D microstructure of the healthy non-human primate lamina cribrosa by optical coherence tomography imaging. *Transl Vis Sci Technol*. 2022;11(4):15.
17. Domander R, Felder AA, Doube M. BoneJ2 - refactoring established research software. *Wellcome Open Res*. 2021;6:37.
18. Glidai Y, Lucy KA, Schuman JS, et al. Microstructural deformations within the depth of the lamina cribrosa in response to acute in vivo intraocular pressure modulation. *Invest Ophthalmol Vis Sci*. 2022;63(5):25.
19. Inui M, Umezu N, Wakasaki K, Sato S. Thickness and clearance visualization based on distance field of 3D objects. *J Comput Des Eng*. 2015;2(3):183–194.
20. Richert C, Odermatt A, Huber N. Computation of thickness and mechanical properties of interconnected structures: accuracy, deviations, and approaches for correction. *Front Mater*. 2019;6:327.
21. Hildebrand T, Rüegsegger P. A new method for the model-independent assessment of thickness in three-dimensional images. *J Microsc*. 1997;185(1):67–75.
22. Lockwood H, Reynaud J, Gardiner S, et al. Lamina cribrosa microarchitecture in normal monkey eyes part 1: methods and initial results. *Invest Ophthalmol Vis Sci*. 2015;56(3):1618–1637.
23. Reynaud J, Lockwood H, Gardiner SK, Williams G, Yang H, Burgoyne CF. Lamina cribrosa microarchitecture in monkey early experimental glaucoma: global change. *Invest Ophthalmol Vis Sci*. 2016;57(7):3451–3469.
24. Wang B, Nevins JE, Nadler Z, et al. In vivo lamina cribrosa micro-architecture in healthy and glaucomatous eyes as assessed by optical coherence tomography. *Invest Ophthalmol Vis Sci*. 2013;54(13):8270–8274.
25. Ivers KM, Sredar N, Patel NB, et al. In vivo changes in lamina cribrosa microarchitecture and optic nerve head structure in early experimental glaucoma. *PLoS One.* 2015;10(7):e0134223.
26. Vilupuru AS, Rangaswamy NV, Frishman LJ, Smith EL, 3rd, Harwerth RS, Roorda A. Adaptive optics scanning laser ophthalmoscopy for in vivo imaging of lamina cribrosa. *J Opt Soc Am A Opt Image Sci Vis*. 2007;24(5):1417–1425.
27. Omodaka K, Maekawa S, An G, et al. Pilot study for three-dimensional assessment of laminar pore structure in patients with glaucoma, as measured with swept source optical coherence tomography. *PLoS One*. 2018;13(11):e0207600.
28. Fontana L, Bhandari A, Fitzke FW, Hitchings RA. In vivo morphometry of the lamina cribrosa and its relation to visual field loss in glaucoma. *Curr Eye Res*. 1998;17(4):363–369.
29. Nouri-Mahdavi K, Hoffman D, Tannenbaum DP, Law SK, Caprioli J. Identifying early glaucoma with optical coherence tomography. *Am J Ophthalmol*. 2004;137(2):228–235.